Heliyon 5 (2019) e01859

Contents lists available at ScienceDirect

Heliyon

journal homepage: www.heliyon.com

Phosphorus as a promoter of a nickel catalyst to obtain 1-phenylethanol from chemoselective hydrogenation of acetophenone

Dolly Carolina Costa [a], Analía Leticia Soldati [b], José Fernando Bengoa [a], Sergio Gustavo Marchetti [a], Virginia Vetere [a,*]

[a] Centro de Investigación y Desarrollo en Ciencias Aplicadas "Dr. Jorge J. Ronco"-CINDECA (UNLP-CONICET-CICBA), Calle 47 N 257, 1900, La Plata, Bs. As, Argentina
[b] Grupo de Caracterización de Materiales, Centro Atómico Bariloche, CONICET. Av. Bustillo, 9500, San Carlos de Bariloche, Río Negro, Argentina

ARTICLE INFO

Keywords:
Materials chemistry
Organic chemistry
Physical chemistry
Chemical engineering
Materials science
Nanoparticles
Metallic nickel
Nickel phosphides
Hydrogenation
1-Phenylethanol

ABSTRACT

Two catalysts were prepared using monodisperse pre-synthetized nanoparticles of metallic nickel and nickel phosphides with the same average diameter. Both nanoparticles species were deposited on the same support: mesoporous silica nano-spheres of MCM-41. This support is suitable to inhibit agglomeration and sintering processes during preparation steps. Therefore, two supported and activated catalysts with the same average nanoparticles diameter were obtained. They differ only in the nature of the active species: metallic nickel and nickel phosphides. The effect of the presence of a second element (phosphorus), more electronegative than nickel, on the activity and selectivity in the chemoselective hydrogenation of acetophenone was studied. The reaction conditions were: H_2 pressure of 1 MPa, 80 °C using n-heptane as solvent. With the aim to understand the catalytic results, nanoparticles, support and catalysts were carefully characterized by X-ray diffraction, diffuse light scattering, transmission electron microcopy, high resolution transmission electron microcopy, selected area electron diffraction, scanning electron microcopy, Fourier transformer infrared spectroscopy, N_2 adsorption at -196 °C, atomic absorption, H_2 and CO chemisorption and volumetric oxidation. Considering these results and geometric and electronic characteristics of the surface of both active species, a change in the adsorption intermediate state of acetophenone in presence of phosphorus is proposed to explain the hydrogenation chemoselectivity of nickel phospides.

1. Introduction

Selective hydrogenations of aromatic ketones into the corresponding alcohols are commonly performed by homogeneous catalysis. However, these processes have economic and environmental disadvantages. Taking into account the key role of this type of alcohols in the fine chemical industries (and especially pharmaceuticals), great efforts are performed in order to replace homogeneous by heterogeneous catalysis, achieving an adequate activity and selectivity. In order to produce the hydrogenation of aromatic ketones, noble metals as Pd, Pt, Rh and Ru are commonly used as catalysts. Several items, such as metal and support selection, metal precursor, catalyst preparation and activation methods, particle size, etc., have strong influence on activity and selectivity in these types of reactions [1, 2, 3, 4]. However, these metals have several disadvantages: high cost, low abundance and low selectivity produced by different kind of side reactions such as the aromatic ring hydrogenation, as well as hydrogenolysis of our valuable product, the intermediate aromatic alcohol. With the purpose of increasing selectivity, a second metal is added. These promoters can modify the noble metal either electronically and/or geometrically [5]. Specifically, a decrease in their hydrogenating capacity is required to achieve an increase in selectivity towards the desired product. The promoters used such as Ni, Cr and Sn, are more electropositive than the noble metal [6, 7, 8, 9]. They produce a double effect: the noble metal gets a negative charge density, Meδ-, and the active sites are diluted, consequently the hydrogenating capacity is decreased. Besides, these electronic and geometric rearrangements in the active site could produce changes in the adsorption mode of the substrate increasing the selectivity towards the desired product. However, this methodology normally leads only to an enhancement, but not a complete change in selectivity.

More recently, with the advancement of nanotechnology, the chemoselective hydrogenations with nanomaterials of transition metals, such as Ni and Fe (cheaper, abundant and less toxic metals), have begun to be explored [10]. Primarily, these reports have analyzed the

* Corresponding author.
E-mail address: vetere@quimica.unlp.edu.ar (V. Vetere).

https://doi.org/10.1016/j.heliyon.2019.e01859
Received 6 February 2019; Received in revised form 21 May 2019; Accepted 28 May 2019

hydrogenation of α,β-unsaturated compounds such as acrolein and cinnamaldehyde but not of aromatic ketones. Besides, the use of pure nickel as catalyst in hydrogenation of cinnamaldehyde, both in gas and liquid phases, leads to production of hydrocinnamaldehyde [11, 12, 13]. It is well known that the hydrogenation of C=C bond is both thermodynamically and kinetically favored over the C=O bond, due to the lower C=C dissociation enthalpy (611 kJ/mol) than for C=O bond (737 kJ/mol) [14]. Therefore, these results do not represent examples of chemoselective hydrogenations in order to obtain the more interesting product: the cinnamyl alcohol. Subsequently, Malobela et al. studied the effect of nickel dispersion and they found that the turnover frequency and the selectivity to unsaturated alcohol increased when the nickel crystal size decreased in the following order: 14.5 nm < 7.8 nm < 2.8 nm [15]. In agreement with these results, Viswanathan et al. reported the cinnamyl alcohol production using Ni/TiO_2 catalysts prepared by four different methods. The catalysts with the smallest nickel particle size, showed the higher cinnamaldehyde conversion and selectivity to cinnamyl alcohol [16]. On the other hand, there are only reports of hydrogenation of aromatic aldehydes and imides, which were transformed into the corresponding alcohols or amines, using iron nanoparticles supported on polymers and molecular H_2 as hydrogenating agent [17].

With the aim to prepare catalysts based on nickel, some compounds could be more appropriate to perform chemoselective hydrogenation of aromatic ketones, than the pure nickel. These substances should preserve nickel metallic characteristics, have moderate hydrogenation capacity and catalytic sites with particular geometries. Therefore, the spatial configuration of the adsorbed molecules and the structural characteristics of the catalytic sites would allow to "tune" the proper arrangement to reach the desired hydrogenation. Taking into account these concepts and considering that in last years, nickel phosphides catalysts have emerged as excellent hydrotreating catalysts [18, 19, 20, 21], they can have good activity in hydrogen transfer reactions, such as chemoselective hydrogenations. Nickel phosphides have metallic properties, the phosphorus presence produces a diluting effect on the Ni atoms, and they have a wide range of stoichiometries, from Ni_3P to NiP_3. Because of these different compositions, they have a great diversity of crystallographic structures, which produce surface sites with very diverse geometries. Therefore, there could be catalytic sites, with geometries that could be able to hydrogenate different aromatic ketones to obtain the desired products.

The use of nickel phosphides as chemoselective hydrogenation catalysts in the fine chemical area is scarce and it has not been applied for hydrogenation of aromatic ketones. As an example of chemoselective hydrogenation of other type of molecules using nickel phosphide as catalyst, Carenco et al. [22] reported good conversion of terminal and internal alkynes to cis-alkenes with high selectivity using nanoparticles of Ni_2P.

From a complete analysis of the previous topics present work explores the possible promoter effect produced by the presence of phosphorus atoms in nickel phosphides when they are used in chemoselective hydrogenation of an aromatic ketone. We decide to study this effect on the activity and selectivity in the chemoselective hydrogenation of acetophenone (AP) to obtain 1-phenylethanol. This is a very important intermediate aromatic alcohol in the fine chemical industry and is conventionally produced by this reaction [23]. Is interesting to remark that the promoting effect on the noble metals is achieved adding a second more electropositive metal (Ni, Cr, Sn). In this case, if nickel phosphides are used as catalysts, phosphorus atoms are more electronegative than Ni. Therefore, a positive charge density on Ni atoms (Niδ+) should be expected. As a consequence, a contrary effect with respect to previous studies would be awaited. Recently, we have published results indicating that nickel phosphides nanoparticles of 9 nm are active as chemoselective hydrogenation catalysts of an aromatic ketone [24]. To our knowledge, this is the first report on this application until now. In the present work, the hydrogenation results obtained with nanoparticles of pure metallic nickel and nickel phosphides of very similar crystal size (≅ 20 nm) are compared.

Considering that these type of reactions are structure sensitive [16, 17] both catalysts were prepared with monodisperse nanoparticles (NPs) pre-synthesized with the same average diameter. In this way, the catalytic results will show the specific effect of the electronic and structural differences between the metallic nickel and the nickel phosphides, without the influence of different sizes of active NPs. After the obtaining and purification of the NPs, they are supported on mesoporous silica nanospheres of about 500 nm and are used as catalysts in the hydrogenation of AP in liquid phase.

2. Experimental

2.1. Nanoparticles synthesis

In a one-pot synthesis to obtain Ni^0 NPs, determined amounts of nickel (II) acetylacetonate $(Ni(acac)_2$, 1 mmol, Sigma-Aldrich, 98%), trioctylphosphine as ligand (TOP, 0.8 mmol, Sigma-Aldrich, 97%), oleylamine as solvent and reducing agent (OA, 10 mmol, Sigma-Aldrich, 70%) were directly added into a three-neck round bottom flask fitted with a condenser and magnetic stirring. The two remaining necks were used to introduce a thermocouple with a glass sheath and Ar flow, respectively. The mixture was heated at 220 °C for 2 h. Finally, the NPs were purified and isolated precipitating the suspension with acetone and re-dispersed in n-hexane.

In order to obtain nickel phosphide NPs, the same procedure was used but TOP was replaced by triphenylphosphine, acting as ligand and phosphorus source (Ph_3P, 0.4 mmol, Sigma Aldrich, 99%).

The NPs were characterized by X-ray diffraction (XRD), diffuse light scattering (DLS), transmission electron microcopy (TEM), selected area electron diffraction (SAED) and Fourier transformer infrared spectroscopy (FT-IR). Atomic absorption spectroscopy (AA) was used to determine the Ni content in the suspension and in catalysts. In this work only the characterization of Ni^0 NPs will be reported, because nickel phosphides characterizations were previously described [24].

2.2. Support synthesis

Ordered mesoporous silica nanospheres (MSNS) were prepared following the methodology proposed by Grün et al. [25] using tetraethyl orthosilicate (TEOS ≥99 %, Aldrich) as silica source, n-hexadecyltrimethylamonnium bromide (CTMABr ≥98 %, Sigma) as template agent, NH4OH (28 % p/p, Merck) to generate an alkaline medium, absolute ethanol (Cicarelli, 99.5 %) and distilled water. All reactants were mixed under vigorous magnetic stirring using the following molar composition: 1TEOS: 0.3CTMABr: 11NH4OH: 58 EtOH: $144H_2O$. The reaction mixture was kept under stirring at 30 °C for 2 h. The precipitate was collected by vacuum filtration and washed with distilled water. The sample was calcined up to 550 °C in air atmosphere for 2 h, with a heating rate of 10 ºC/min in order to remove the CTMABr. The solid was characterized by N_2 adsorption at -196 °C, scanning electron microscopy (SEM) and TEM.

2.3. Catalyst preparation

The Ni^0 and nickel phosphides NPs catalysts were prepared by impregnation of silica nanospheres with the corresponding presynthetized NPs suspensions and dried at 60 °C in air during 2 h. They were called Ni-MSNS and NiP-MSNS, respectively. The volume suspensions was fixed in order to obtain a nominal Ni loading of 5 % wt/wt.

With the purpose to eliminate the surfactants (TOP or Ph_3P) from the surface of the NPs, both solids were washed three times with $CHCl_3$. The catalysts were characterized by TEM. Before their use in the reaction, they were reduced in H_2 flow, heating at 10 ºC/min up to 500 °C and maintaining at this temperature during 2h. Afterwards, TEM micrographs were obtained in order to verify that the reduction treatment did not produce sintering of the NPs.

The number of the catalytic surface sites of Ni-MSNS and NiP-MSNS was titrated by H_2 and CO chemisorption, respectively. Besides, the volumetric oxidation technique was used to evaluate the oxygen total quantity needed to re-oxidize the reduced Ni-MSNS catalyst.

2.4. Characterizations

XRD patterns were recorded using a standard automated powder X-ray diffraction system (Philips PW170, the Netherlands) with diffracted-beam graphite monochromator, using Cu Kα radiation (λ = 0.15406 nm) in the range 2θ = 30-80° with steps of 0.05° and counting time of 6 s/step. Besides, a diffractogram of MCM-41 nanospheres at low angles (2θ = 1.0–10.0°) was obtained with laboratory beamline Xenocs (Model Xeuss 2.0, France). This equipment has the capability to run simultaneous small and wide-angle X-ray scattering measurements (SAXS-WAXS). The present test was made in WAXS mode.

The size distribution of the Ni NPs in suspension was obtained with a Zetasizer Nano (Nano ZSizer-ZEN3600, Malvern, U.K.) commercial equipment at room temperature. The light source was a helium/neon laser (λ = 632.8 nm) and the light scattering was measured at scattering angle of θ = 173°.

A Philips CM 200 UT microscope (the Netherlands) equipped with an ultra-twin objective lens was used to obtain the TEM and HRTEM (high resolution transmission electron microscopy) images. A LaB_6 filament operated at 200 keV was the electron source. In the high-resolution mode, the nominal resolution was of 0.2 nm. The micrographics were acquired with a CCD digital camera. A commercial program for image treatment was used to adjust linearly the illumination and contrast. Besides, electron diffraction of selected area (SAED) was obtained. Statistics on particles were done with the program Image J 1.43U. Particle size is given as the geometric average size ±standard deviation of the largest particle dimension. In all cases, more than 100 measurements were averaged, sampling in different regions of the sampler holder.

A Philips 505 (the Netherlands) microscope was used for SEM analysis.

A FT/IR Jasco spectrometer (model 4200, Japan) equipped with a PIKE diffuse reflectance IR cell with a resolution of 1 cm^{-1} was used. From 200 to 400 scans were accumulated in each case.

Textural properties as specific surface area (S_g), specific pore volume (V_p) and pore diameter (D_p) of MSNS were measured with a Micromeritics ASAP 2020 V1.02 E device (U.S.A.).

Measurements of the surface Ni atoms were made on the catalysts in conventional static volumetric handmade equipment. Both isotherms were measured at 50 °C, with H_2 as titration reactant for Ni-MSNS and CO for NiP-MSNS. Before acquisition of isotherms, the catalysts were reduced *in situ* as it was previously described. After H_2 chemisorption test, Ni-MSNS catalyst was degassed and completely oxidized with a known amount of pure O_2.

2.5. Catalytic tests

AP hydrogenation reaction was carried out in a stirred autoclave reactor at 1MPa H_2 pressure and 80 °C, using 0.25 g catalyst and n-heptane as solvent. Before the catalytic test, the solids were activated in pure H_2 following the procedure already described. The operative conditions for the catalytic tests were specifically chosen to avoid mass transfer control. The reaction evolution was followed by gas chromatography in a GC Varian 3400 chromatograph (the Netherlands) equipped with a capillary column of 30 m CP wax 52 CB and FID. The identification of reaction products was accomplished by GC/MS using Shimadzu QP5050 equipment (Japan).

3. Results and discussion

The characterization of nickel phosphide NPs was previously reported [24]. Briefly, a mixture of $Ni_{12}P_5$ and Ni_2P NPs was obtained, where each NP is monophasic. The major phase is $Ni_{12}P_5$. About of 87% molar of the mixture corresponds to this compound. In this article the geometric average size of the NPs, determined by TEM, was of 9.6 ± 0.2 nm. In the present work the molar ratio of reactants: Ni(acac)2: OA: Ph3P was modified, decreasing the Ph3P quantity from 0.8 to 0.4 mmol, while quantities of Ni(acac)2 and OA were maintained equal. This change was performed in order to obtain NPs with an average diameter similar to that of the Ni0 NPs. In this way, an average value of 15.1 ± 0.6 nm was obtained by TEM. As it will be explained below, this size is nearly equal to the diameter of the Ni0 NPs. Therefore, possible effects of the NPs sizes on activity and selectivity of the catalysts should be avoided [2].

In Fig. 1 XRD diffractogram of the Ni NPs, with peaks at 2θ = 44.3, 51.3 and 76.4° is shown. The position of the three peaks are in good agreement with (1 1 1) (2 0 0) and (2 2 0) crystallographic planes of a face-centered cubic (f.c.c.) unit cell, typical of metallic Ni [PDF 88–2326]. The broadening of the diffraction peaks is characteristic of very small NPs. At first sight, the presence of nickel oxide phase cannot be ruled out completely because the strongest peak of NiO appears at 2θ = 43.3° [PDF 89–7390]. Due to the considerably broadening of the Ni0 peaks, could be possible that the left side of 44.3° signal hidden a very small peak of NiO. However, the absence of any distinguishable peak at other characteristic positions of nickel oxide, such as 2θ = 37°, indicates that the presence of this phase is negligible. Therefore, we can conclude that the synthesis procedure used led to the obtaining of Ni0 NPs.

In order to obtain information about the average size diameter and the monodisperse character of the Ni^0 NPs distribution, DLS measurements were performed. They are easily and quickly performed and provide significant statistical information. However, this technique measures the hydrodynamic diameters, this mean, the real NPs diameters plus the thickness of the NPs coverage. Depending on the difference of the refractive indexes between the solvent used in the suspension and the NPs surfactant, a significant or a negligible disagreement, in comparison with the real diameter, can be observed [26]. The results obtained by this technique show that the Ni^0 NPs suspension is monodisperse (polydispersity index <0.06) and they have an average diameter of 19 ± 6 nm.

The Ni^0 NPs were characterized using TEM and SAED techniques (Fig. 2 A and B). Fig. 3 show the histogram obtained counting 115 NPs. It was fitted using a log-normal distribution considering that particles lower than 20 nm present this class of size distribution [27]. The statistical parameters obtained from the fitting showeda geometric average diameter of 16.0 ± 0.2 nm. Comparing this value with that obtained by DLS, and considering the standard error, there is a good agreement between both techniques. In order to confirm that the NPs obtained are of Ni^0, the SAED was acquired and analyzed. The lattice spacings measured from the rings of the diffraction pattern (Fig. 2B) were: 0.200, 0.167 and

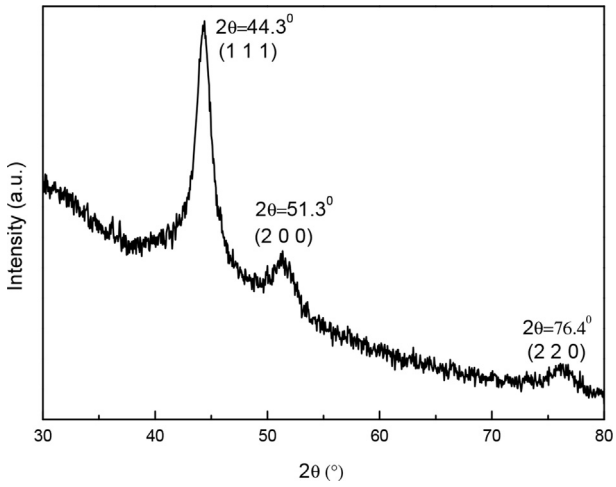

Fig. 1. XRD diffractogram of the Ni^0 NPs.

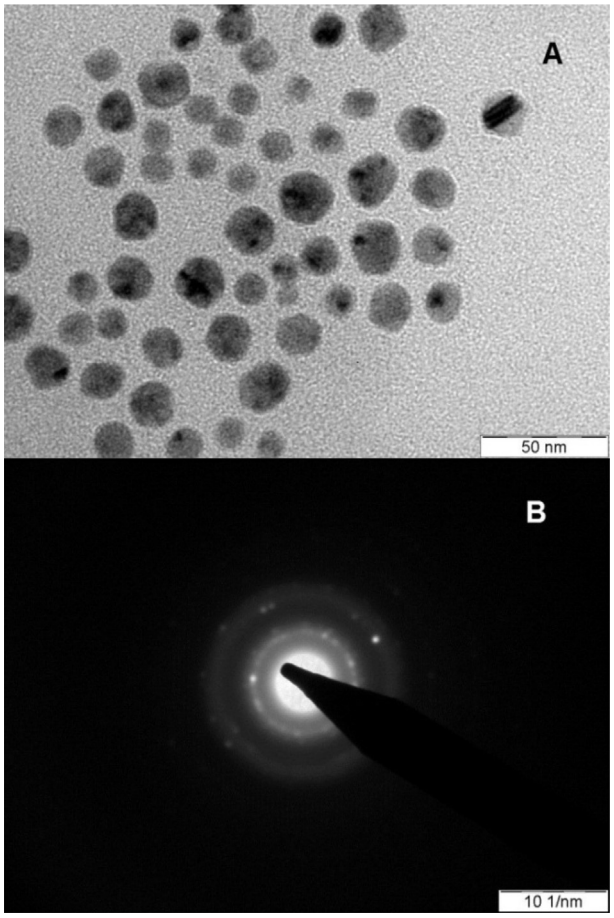

Fig. 2. TEM (A) and SAED (B) images of the Ni^0 NPs.

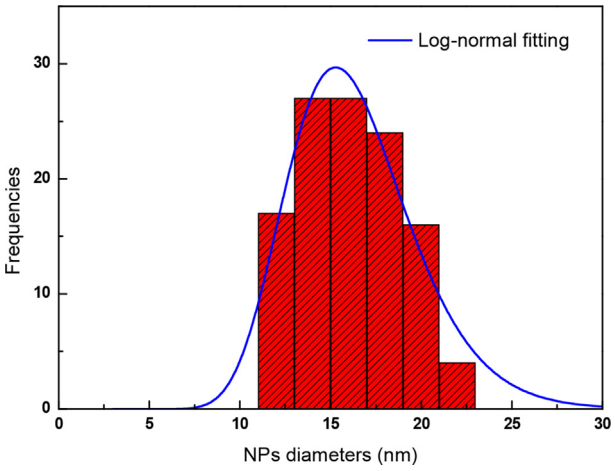

Fig. 3. Histogram of the Ni^0 NPs sizes obtained from TEM. Blue line was obtained fitting the results assuming a log-normal distribution.

0.118 nm. They are in very good agreement with the known lattice spacings for Ni^0 bulk: 0.199, 0.173 and 0.122 nm. Therefore, this technique confirms the assignment performed by XRD.

To determine if the OA and TOP remain on the NPs surface, the FT-IR spectrum was obtained (Fig. 4). The NPs suspension was mixed with KBr mechanically and then dried. This procedure was performed in order to avoid the overlapping of the support bands with the ones belonging to OA and TOP. In Table 1 are shown the detected peaks and its assignations. The bands corresponding to symmetric and asymmetric stretching vibrations of (C–H) and bending vibration of (CH_3) can be assigned to the

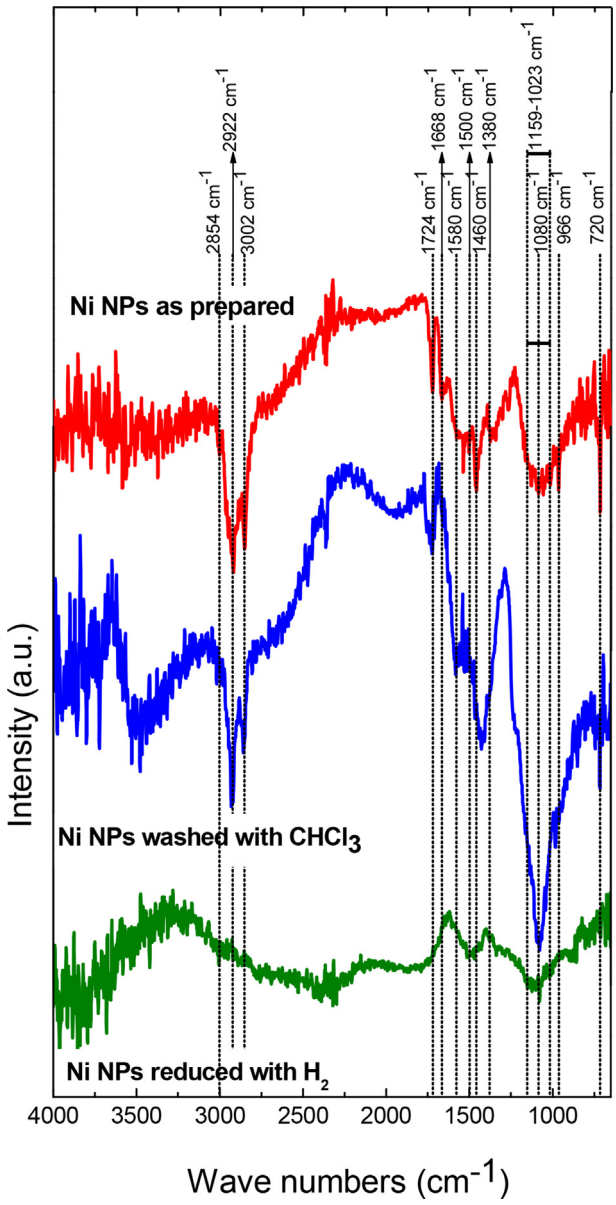

Fig. 4. FTIR of Ni NPs as prepared (red spectrum), washed with $CHCl_3$ (blue spectrum) and reduced with H_2 (green spectrum).

Table 1
Assignments of the FTIR bands detected in the as prepared NPs.

Wave number (cm^{-1})	Vibrational modes*	Assigned to	Reference
3002	δ(=C–H)	OA	[20]
2922, 2854	νas (C–H) and νs (C–H)	OA/TOP	[20, 21, 22]
1724	ν(C=O)	(OA + acac)	[24]
1668	δ(-C=C)	OA	[20]
1580	δ(-N-H)	OA	[23]
1500	δ(CH3)	TOP	[21]
1460	δ(CH3)	OA/TOP	[20, 21]
1380	δ(CH3)	TOP	[21]
1159–1023	ν(C–P)	TOP	[22]
1080	Ni–P=O	Oxidation of TOP	[16]
966	δ(=C–H)	OA	[23]
720	ν (–CH2–)n (n ≥ 4)	OA/TOP	[21]

*νs = symmetric stretching vibration; νas = asymmetric stretching vibration; δ = bending vibration.

alkyl groups of OA and TOP [28, 29, 30]. It is no possible to distinguish between both compounds from these signals. However, the bending vibrations of (=C–H) (-C=C) and (-N-H) are exclusive of OA, and their presence on the NPs surface could be confirmed [28, 29, 30, 31]. On the other hand, the presence of other bending bands (CH_3) and various stretching (C–P) bands in the range of 1159–1023 cm^{-1} indicates that TOP is also adsorbed on the surface of Ni NPs [29, 30]. The stretching peak of the carbonyl group at 1724 cm^{-1} appears as a consequence of the reaction between OA and acetylacetonate groups [32]. Finally, the band at 1080 cm^{-1} could be assigned to the stretching -P=O bonded at a surface nickel atom [33]. These species would be produced by TOP oxidation during the purification process of the NPs and its handling to prepare the sample to obtain the FTIR spectrum, because these steps were performed in air atmosphere.

A similar result was found with the nickel phosphide NPs, but instead of TOP, Ph_3P was detected on the surface [24].

The silica support obtained is made of nanometric spheres of an average diameter of 530 ± 8 nm with interparticular channels. In Fig. 5A a SEM micrograph is shown. In order to estimate the average value of these channels, the textural properties of MSNS before calcination were measured. The values obtained were: BET specific surface area: 17 m^2/g,

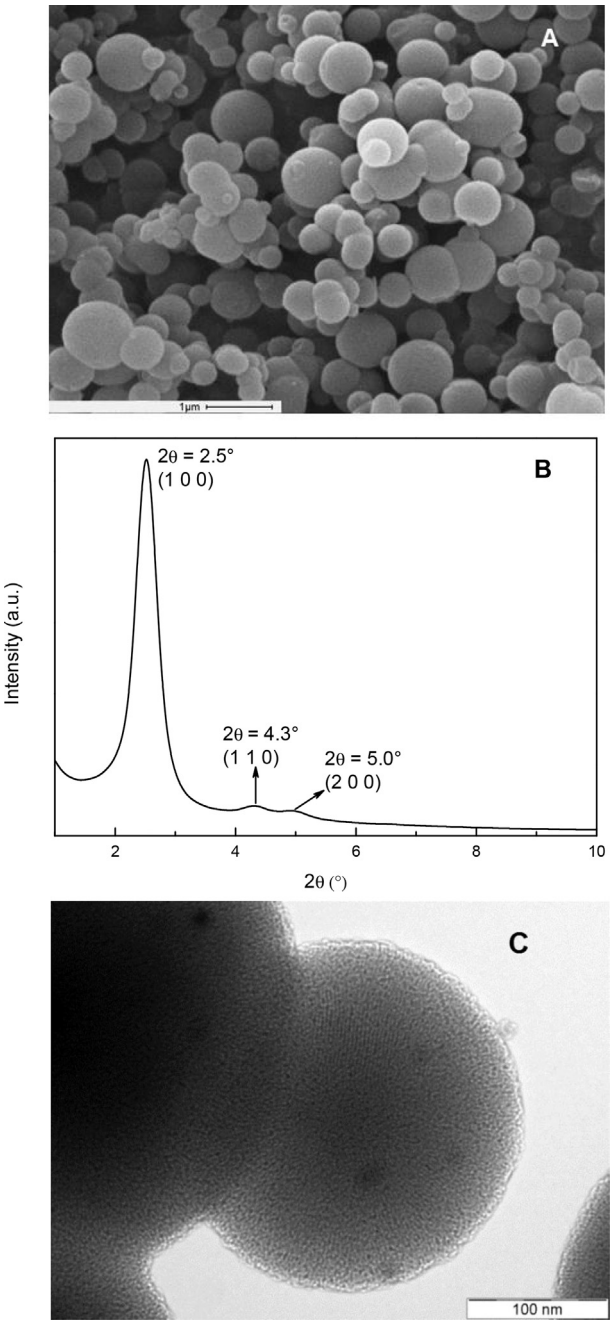

Fig. 5. Nanometric spheres of silica support. SEM micrograph (A), XRD at low angles (B) and TEM image (C).

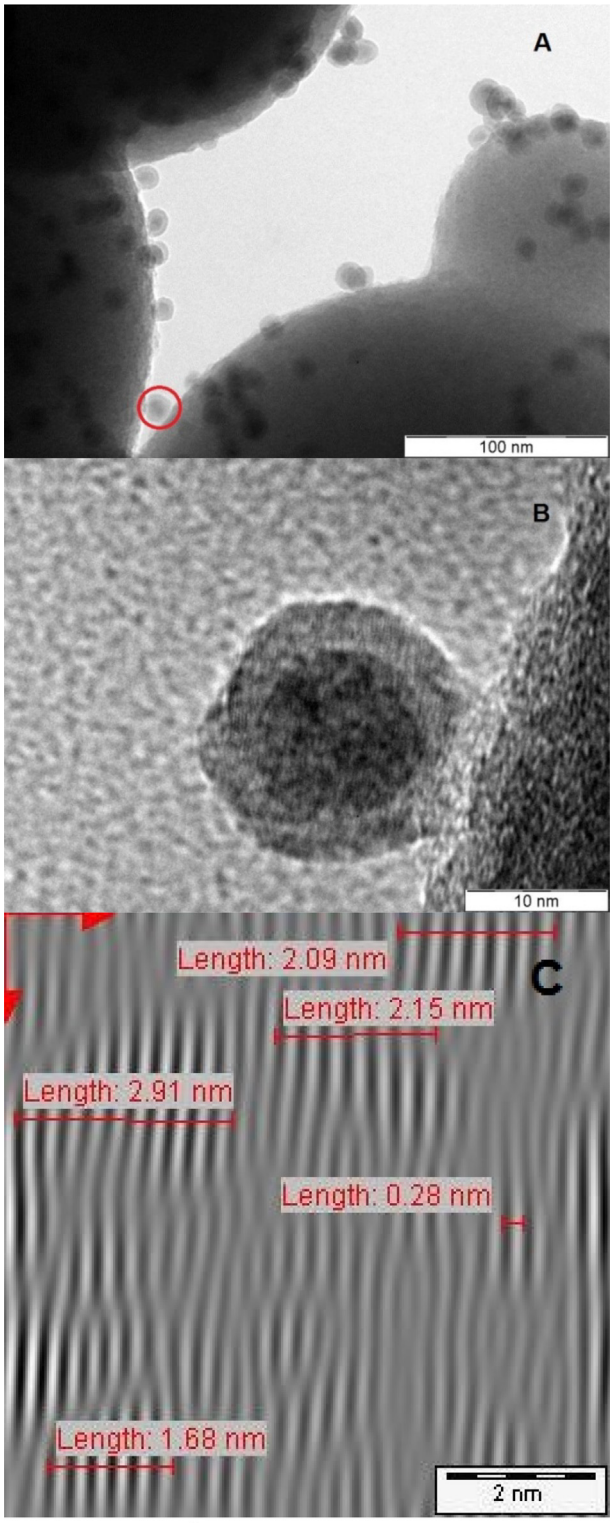

Fig. 6. TEM micrographs of Ni^0 NPs supported on MSNS by impregnation method (A), HRTEM of an isolated nanoparticle (B) and their inverse Fourier transform (C).

average pore diameter, from BJH method: 10 nm and pore volume: 0.02 cm^3/g. After calcination these values were: BET specific surface area: 1067 m^2/g, average pore diameter: 2 nm and pore volume: 0.6 cm^3/g. The textural values of the MSNS after calcination were typical of a mesoporous ordered silica (MCM-41). The hexagonal ordering was checked by XRD at low angles (Fig. 5B). Besides, in TEM image (Fig. 5C) this arrangement can be observed. It must be highlighted that the presence of the mesopores typical of MCM-41 (about of 2 nm of diameter) are not useful to locate Ni^0 and nickel phosphides NPs inside of them because of steric hindrance. However, the CTMABr must be added within the gel synthesis in order to obtain the SiO_2 nanospheres. On the other hand, as it can be seen in the SEM micrograph, there are interparticular macropores with different sizes depending on the nanospheres packing. The sizes of these macropores change from 90 × 80 nm to 450 × 400 nm. The nanospheres and the macropores between them afford the adequate support to anchorage the NPs, as we will describe below.

The silica support was impregnated with Ni^0 and nickel phosphides pre-synthetized NPs suspensions, respectively. As it can be seen in TEM micrographs neither agglomeration nor changes in NPs size were detected (Fig. 6A and reference [24]). As it can be seen in Fig. 6A, Ni^0 NPs are located preferentially on the surface of the SiO_2 nanospheres, but some of them are placed inside the interparticular pores (one of them is highlighted with a red circle). The Ni loadings of both systems, determined by AA, are shown in Table 2.

The HRTEM analysis of the supported Ni^0 NPs shows that they have a "core-shell" structure (Fig. 6B). A "shell" thickness of about 3.5 nm was measured in the micrograph. On the other hand, using the inverse Fourier transform of HRTEM images of this "shell", an average lattice spacing of 0.27 nm was obtained (Fig. 6C). As a consequence of the small thickness of this "shell", few diffraction points can be selected to produce the inverse Fourier transform. Therefore, not many crystalline distances can be measured in order to obtain an average value. In spite of these constraints, clearly the value of 0.27 nm cannot be assigned to Ni^0. Instead, it has a good coincidence with (1 1 1) diffraction plane of NiO with f. c.c. crystalline structure. This is an interesting result because we must remember that the surface of the NPs is covered with OA and TOP. Therefore, during solvent elimination (hexane) at 60 °C in air, this layer of organic molecules cannot inhibit the approach of atmospheric O_2, leading to the NiO "shell" production.

Considering the previous results, before using the supported NPs as catalysts, two processes were necessaries. In both catalysts the organic layer (phosphorous oxidized species -P=O) was eliminated by washing and reducing with hydrogen flow. This last treatment also eliminated the NiO "shell" in the catalyst with Ni^0 NPs.

To perform the first step, three washes of the supported catalysts with $CHCl_3$ were done, following the method proposed by Senevirathne et al [33]. In order to check the efficiency of the procedure, the same mixture of (Ni^0 NPs + KBr) used to obtain the FT-IR spectrum of Fig. 4, was washed with $CHCl_3$ and a new FT-IR spectrum was obtained. In Fig. 4 it can be seen that, this treatment partially eliminates the OA. In this way, the δ(-C=C) band have disappear completely, but the other bands are visible yet. On the other hand, all bands assigned to TOP were clearly detected. This result proves that the adsorption of TOP is stronger than that of OA on the Ni^0 NPs surface.

Considering that we used the same sample, the peak intensities between non-washed and washed sample can be qualitatively compared. As consequence, it can be concluded that the band assigned to the stretching -P=O, bonded at a surface nickel atom, increase its intensity in a significant way after washing with $CHCl_3$. Therefore, handling the sample in air atmosphere, increase TOP oxidation.

After the partial elimination of the organic layer both systems: Ni-MSNS and NiP-MSNS were reduced as it was previously described. In Fig. 7A, the micrograph reveals that Ni^0 NPs sintering did not occur during this treatment. On the other hand, in Fig. 7B and C HRTEM image of one Ni^0 NPs and their corresponding inverse Fourier transform are shown. Because of the reduction treatment is evident that the "core-shell" structure disappeared and the crystalline spacing determined by inverse Fourier transform (Fig. 7C) is of 0.23 nm. Clearly, this value is lower than that assigned to (1 1 1) diffraction plane of NiO with f. c.c. crystalline structure (Fig. 6C).

On the other hand, it is higher than Ni^0 spacing assigned to (1 1 1) planes. There are several reports in which an increasing of the interplanar distances in NPs, in comparison with the bulk value, has been detected. Thus, Winnischofer et al. [34] found a shifting to higher value crystalline spacing for the (1 1 1) plane in Ni^0 NPs with f. c.c. crystalline structure. These authors considered that, most of the metals with f. c.c. crystalline structure and nanometric sizes, exhibit axes with five-fold symmetry. This kind of structure is forbidden in bulk crystals and led to NPs with icosahedral or decahedral shapes. These types of particles are known as "multiply-twinned particles", and this structural distortion would produce the increasing of the interplanar distances.

On the other hand, the same mixture of (Ni^0 NPs + KBr), used to obtain the FT-IR spectrum after three washes with $CHCl_3$, was reduced using identical conditions to Ni-MSNS. In Fig. 4, the FT-IR spectrum is shown. Weak bands at 1500 and 1460 cm^{-1} -corresponding to bending vibrations of (CH_3) groups of TOP- and a wide signal in the range of 1159–1023 cm^{-1} -assignable to stretching of (C–P) bonds of TOP- were detected.

Also, the band at 1080 cm^{-1}, corresponding to stretching of -P=O, bonded to a superficial nickel atom, was observed. Strikingly, we can conclude that, after the treatment in pure H_2 flow during 2 h at 500 °C, there are remains of TOP and oxidized TOP on the surface of the Ni^0 NPs. This fact is undesired because both species will block a certain number of active sites.

Table 2 lists the H_2 and CO chemisorption results for the Ni-MSNS and NiP-MSNS, respectively. Besides, the metallic dispersions and the crystallite sizes obtained from the corresponding chemisorption measurements are reported. Assuming that the Ni^0 NPs have a spherical geometry, the particle size can be estimated from the equation $d_{AV} = 101/D$, where d_{AV} represents surface-weighted average crystallite diameter in nm and D the metal dispersion, in % [35]. Using this equation and the metallic dispersion calculated from the H_2 chemisorption value by assuming a stoichiometry of one H atom per surface metallic atom, the Ni NPs size was calculated (Table 2). As it can be seen, this value is approximately five times larger than the size determined by TEM (101 nm vs 19 ± 6 nm, respectively). Clearly, this discrepancy has its origin in

Table 2
Ni loadings, physicochemical and catalytic properties of Ni-MSNS and NiP-MSNS catalysts.

Catalyst	Ni% (wt/wt)	Chemisorption (μmol/g cat)		D[a] (%)	d_{AV}[b] (nm)	Volumetric oxidation (μmol/g cat)	R[c] (%)	X_{AP}[d] (%)	TOF[e] (s^{-1})
		H_2	CO						
Ni-MSNS	4.1	3	——	1.0	101	319	91	31	0.0500
NiP-MSNS	4.3	——	62	8.5	13	——		17	0.0006

[a] Metal dispersion.
[b] Surface-weighted average crystallite diameter.
[c] Ni reduction percentage.
[d] Acetophenone conversion at 300 min of reaction time.
[e] Turnover frequency.

the very low H_2 chemisorption value obtained. This experimental fact is coherent with the presence of TOP fragments that remain on the Ni^0 NPs surface, as was detected from FT-IR spectrum. A similar procedure was followed to evaluate the average size of the nickel phosphides NPs from the CO chemisorption result, assuming spherical geometry and applying the equation $d_{AV} = 6nf/\rho L$. Here, f is the weight fraction of the nickel phosphides in the catalyst, n is the average surface metal atom density (atoms/cm^2), ρ is the nickel phosphide density (g/cm3) and L is the metal site concentration obtained from CO chemisorption by assuming one CO chemisorbed molecule per surface metal atom (atoms/gcatalyst) [36]. Bearing in mind that the NPs suspension used to impregnate the support is a mixture of Ni12P5 and Ni2P, where each NPs is monophasic, we used weighted averages ρ and L values considering the molar composition previously mentioned. The density values used were: ρNi12P5 = 7.53 g/cm3 and ρNi2P = 7.35 g/cm3 [37] and the L values were: LNi12P5 = 1.21 × 1015 atoms/cm2 and LNi2P = 1.01 × 1015 atoms/cm2 [38]. As it can be seen in Table 2 there is an excellent agreement between the calculated d value from the CO chemisorption test and that obtained by TEM. From this result, we can conclude that the surface of the nickel phosphides NPs was properly cleaned during the reduction step and the estimation of the surface metallic atoms obtained from CO chemisorption would produce a reliable TOF number for the catalytic reaction.

On the other hand, we can determine from volumetric oxidation test that a very high percentage of Ni reduction was reached in Ni-MSNS catalyst (Table 2). Probably, the small non-reduced quantity remains as Ni^{2+} diffused inside the walls of the SiO_2 support. This process could occur as consequence of the strong interaction between the NiO "shell" of the NPs and the SiO_2 support. During the reduction step two parallel and competitive processes could take place: the NiO reduction and the diffusion of Ni^{2+} ions inside the SiO_2 lattice. The first step would be predominant and a 91 % of the total Ni loading is reduced to metallic state.

Table 2 shows that, Ni-MSNS catalyst reached the higher AP conversion at 300 min of reaction time with a value of 31 %. At this time, NiP-MSNS only reach 17 % of conversion. Notwithstanding, after 420 min the conversion value of this catalyst is 27 %. Therefore, the AP hydrogenation process takes place more slowly in the catalyst with nickel phosphide NPs. The phosphorus atoms that surround the nickel atoms would produce a diluting effect on the nickel assembly, decreasing the hydrogenation velocity. The corresponding TOF numbers evaluated at 300 min (Table 2) reflects this experimental fact. Is important to remark two aspects about the TOF of Ni-MSNS:

- the presence of TOP fragments on the surface of the Ni^0 NPs could block active sites. Therefore, it is possible that higher conversion could be obtained if a complete elimination of the surfactant could be achieved,
- by the same reason, the quantity of the H2 chemisorbed would be underestimated. As consequence, TOF number would be overestimated.

In order to determine if these catalysts are chemoselective to hydrogenate the carbonyl group of the AP to produce 1-phenylethanol, the selectivities at the same level conversions (about 30 %) were evaluate (Fig. 8). Both catalysts have a very high selectivity to this product. We will analyze these results taking into account the two possible adsorption modes of carbonyl groups on the surface of metal transitions: η^1(O) and η^2(C,O). For AP hydrogenation with a Pt/SiO_2 catalyst, Chen et al. [39] proposed that in η^1(O) mode the coordination happens between the oxygen of the carbonyl group and one metallic site and the aromatic ring remains parallel to the metal surface. Instead, in η^2(C,O) mode, the coordination takes place between π-electrons of C=O and two neighbors surface metallic sites [39]. Considering that the carbon atom of the carbonyl group has sp^2 hybridization, the aromatic ring is tilted with respect to the metallic surface. This configuration would inhibit the phenyl group hydrogenation and high 1-phenylethanol selectivity could

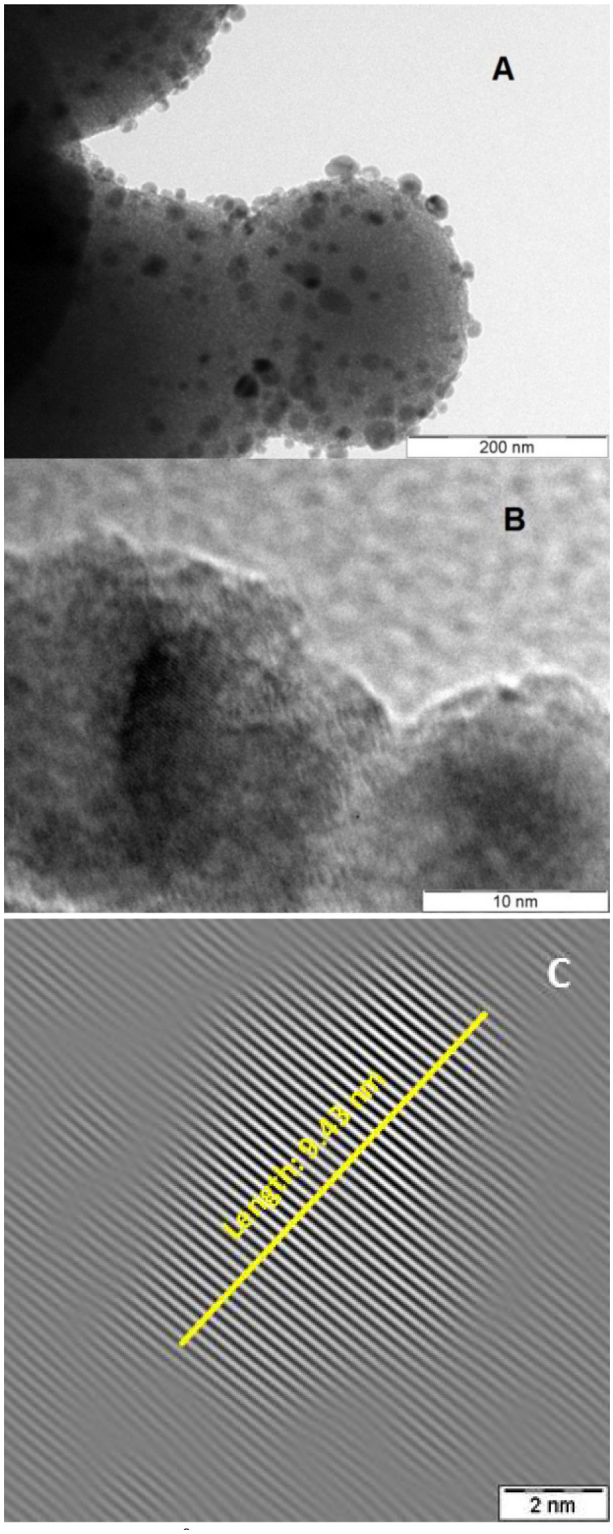

Fig. 7. TEM micrograph of Ni^0 NPs supported on MSNS after reduction treatment (A). HRTEM image of one Ni^0 NPs of this system (B) and their corresponding inverse Fourier transform (C).

be obtained. A similar process would occur with the Ni-MSNS catalyst. Comparing the interatomic Ni–Ni distance (0.249 nm) with the length of the double bond C=O (0.120 nm), in order to get bridge adsorption, the carbonyl bond would be weakened and could be hydrogenated easily.

When nickel phosphides are used as a catalyst to hydrogenate AP some important differences respect to pure metal must be considered.

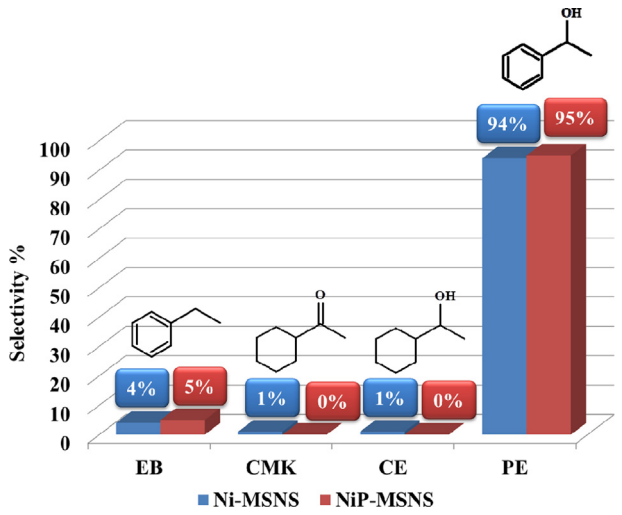

Fig. 8. Selectivity to products in the hydrogenation of AP evaluated at about 30 % of conversion in both catalysts. Reaction conditions:1 MPa of H_2 pressure, temperature: 80 °C and n-heptane as solvent.

Thus, in these phases, P atoms have higher electronegativity than Ni atoms. As consequence, they can be represented as: $P^{\delta-}$ and $Ni^{\delta+}$, respectively. The $Ni^{\delta+}$ surface atoms behave as Lewis acid sites, attracting the atoms with negative charge density of the AP. Besides they work as metallic sites for hydrogenation [40]. Other difference between these compounds and Ni^0, is the presence of charge accumulations along several bonds within the Ni coordination polyhedron surrounding the P atoms as it was demonstrated using the density functional theory [37]. Therefore, it should be unlikely that the AP can be adsorbed in η2(C,O) mode because charge accumulations would repel the π-electrons of C=O. In bibliography has been proposed that the only intermediate of adsorption to produce the hydrogenation of carbonyl molecules, when transition metals are used as catalysts, is η2(C,O) mode [39]. However, considering our experimental results, we assume that when nickel phosphides are used as hydrogenation catalysts, the $Ni^{\delta+}$ surface atoms attract the oxygen of the C=O group and, at the same time, a strong repulsion is produced between the aromatic ring and the negative charge density, accumulated on the surface by the P atoms. As consequence, the bond C=O is weakened, and the hydrogenation is possible but through η^1(O)-like mode as intermediate. Following this train of thought, nickel phosphides could change the mechanism of the chemoselective hydrogenation of the carbonyl group in AP and the intermediate similar to η^1(O) would be reactive to produce 1-phenylethanol. However, this adsorption mode would be less reactive in comparison with η^2(C,O) mode and this would be a second reason (besides the diluting effect produced by phosphorus atoms presence) that would explain the slower hydrogenation with nickel phosphides catalysts with respect to metallic nickel.

4. Conclusions

Monodisperse pre-synthetized NPs of Ni^0 and nickel phosphides with the same average diameter (16.0 ± 0.2 nm vs. 15.1 ± 0.6 nm respectively) were used to prepare two "quasi-model" catalysts. Both NPs species were deposited on nano-spheres of MCM-41 with an average diameter of 530 ± 8 nm. The textural properties of this support were adequate to inhibit agglomeration and sintering processes during impregnating, washing and reduction steps. In this way, we have obtained two supported and activated catalysts with the same average NPs diameter. This structural characteristic allowed performing the comparison of the catalytic results without misleading produced by crystal size effects of the active species.

Both catalysts were tested in hydrogenation of AP and they showed a very similar final conversion of this compound (≅ 30 %) but nickel phosphides present a lower reaction velocity than Ni0. On the other hand, when the selectivities were compared at similar conversion levels (≅ 30 %), in order to avoid some influence of this parameter, both catalysts showed a very high selectivity to 1-phenylethanol (the desired product) of about 95 %. Therefore, we can conclude that the only catalytic difference between both systems would be the hydrogenation reaction velocity. It is necessary to remark that an optimization of the reaction operative conditions was not performed. Thus, it could be possible to get similar reaction velocities if higher reaction temperature is used.

On the other hand, if geometric and electronic surface properties of Ni^0 and nickel phosphides are compared, important differences appear. Thus, the situation with metallic nickel would be similar to other transition metals: AP could be adsorbed through η^2(C,O) mode and the chemoselective hydrogenation occurs successfully. Instead, in nickel phosphides surface there are zones with great negative charge accumulations along some Ni–P bonds. Besides, the electronegativity differences between Ni and P produce charge densities on both atoms: $P^{\delta-}$ and $Ni^{\delta+}$. This complex electronic distribution would produce a strong electrostatic repulsion between some areas of the surface of nickel phosphides and the phenyl group and π-electrons of C=O of the AP. As consequence, we propose that AP only could be adsorbed on top Niδ+ atoms through the oxygen atom of the carbonyl group. That means, the AP would be adsorbed with a mode similar to η1(O) as intermediate. Previous results have shown that through this intermediate, the hydrogenation of the carbonyl group cannot occur if transition metals are used as catalysts. Instead, if nickel phosphides are used, we suppose that the AP would be adsorbed through its oxygen to a $Ni^{\delta+}$ atom but, at the same time, the molecule would be repelled far away from the surface due to the strong electrostatic repulsion generated between them, as it was previously described. In this situation, the C=O bond would be weakened (by a different reason that in the transition metals case) and it could be hydrogenated.

Finally, is interesting to emphasize that nickel phosphides have a very wide range of compositions from Ni_3P to NiP_3. Among them there are great structural and electronic differences which will produce very diverse catalytic sites. Therefore, we could assume that there would be many different organic substrates, with more than one functional group, on which a chemoselective hydrogenation could take place if nickel phosphides, with different stoichiometries, are used. As consequence of these results, we can infer that due to the great versatility of these phases, they appear to be new potential chemoselective hydrogenation catalysts and new attempts to study different compositions and substrates are justified.

Data availability

The raw/processed data required to reproduce these findings cannot be shared at this time as the data also form part of an ongoing study.

Declarations

Author contribution statement

Virginia Vetere: Conceived and designed the experiments; Analyzed and interpreted the data; Wrote the paper.

Dolly Costa: Performed the experiments.

Analia Soldati: Performed the experiments; Contributed reagents, materials, analysis tools or data.

Jose Fernando Bengoa: Performed the experiments; Analyzed and interpreted the data.

Sergio Marchetti: Analyzed and interpreted the data; Wrote the paper.

Funding statement

This work was supported by ANPCyT (PICT N° 00549 and 0148) and Universidad Nacional de La Plata (Projects X757 and X710).

Competing interest statement

The authors declare no conflict of interest.

Additional information

No additional information is available for this paper.

References

[1] P. Kluson, L. Cerveny, Selective hydrogenation over ruthenium catalysts, Appl. Catal. Gen. 128 (1995) 13–31.
[2] V. Ponec, On the role of promoters in hydrogenations on metals; α,β-unsaturated aldehydes and ketones, Appl. Catal. Gen. 149 (1997) 27–48.
[3] P. Gallezot, D. Richard, Selective hydrogenation of α,β-unsaturated aldehydes, Catal. Rev. 40 (1998) 81–126.
[4] P. Mäki-Arvela, J. Hájek, T. Salmi, D.Y. Murzin, Chemoselective hydrogenation of carbonyl compounds over heterogeneous catalysts, Appl. Catal. Gen. 292 (2005) 1–49.
[5] W. Yu, M.D. Porosoff, J.G. Chen, Review of Pt-based bimetallic catalysis: from model surfaces to supported catalysts, Chem. Rev. 112 (2012) 5780–5817.
[6] J. Masson, S. Vidal, P. Cividino, P. Fouilloux, J. Court, Selective hydrogenation of acetophenone on chromium promoted Raney nickel catalysts. II. Catalytic properties in the hydrogenation of acetophenone, determination of the reactivity ratios as selectivity criteria, Appl. Catal. Gen. 99 (1993) 147–159.
[7] R.V. Malyala, C.V. Rode, M. Arai, S.G. Hegde, R.V. Chaudhari, Activity, selectivity and stability of Ni and bimetallic Ni–Pt supported on zeolite Y catalysts for hydrogenation of acetophenone and its substituted derivatives, Appl. Catal. Gen. 193 (2000) 71–86.
[8] M. Casagrande, L. Storaro, A. Talon, M. Lenarda, R. Frattini, E. Rodríguez-Castellón, P. Maireles-Torres, Liquid phase acetophenone hydrogenation on Ru/Cr/B catalysts supported on silica, J. Mol. Catal. A Chem. 188 (2002) 133–139.
[9] G.F. Santori, A.G. Moglioni, V. Vetere, G.Y.M. Iglesias, M.L. Casella, O.A. Ferretti, Hydrogenation of aromatic ketones with Pt- and Sn-modified Pt catalysts, Appl. Catal. Gen. 269 (2004) 215–223.
[10] Hydrogenation with low-cost transition metals, in: J. Sa, A. Srebowata (Eds.), Taylor & Francis Group, 2016.
[11] K.-Y. Jao, K.-W. Liu, Y.-H. Yang, A.-N. Ko, Vapour phase hydrogenation of cinnamaldehyde over nano Ni and Ni/SiMCM-41 catalysts, J. Chin. Chem. Soc. 56 (2009) 885–890.
[12] S.-Y. Chin, F.-J. Lin, A.-N. Ko, Vapour phase hydrogenation of cinnamaldehyde over Ni/γ-Al2O3 catalysts: interesting reaction network, Catal. Lett. 132 (2009) 389–394.
[13] C. Rudolf, B. Dragoi, A. Ungureanu, A. Chirieac, S. Royer, A. Nastro, E. Dumitriu, NiAl and CoAl materials derived from takovite-like LDHs and related structures as efficient chemoselective hydrogenation catalysts, Catal. Sci. Technol. 4 (2014) 179–189.
[14] M.S. Ide, B. Hao, M. Neurock, R.J. Davis, Mechanistic insights on the hydrogenation of α,β-unsaturated ketones and aldehydes to unsaturated alcohols over metal catalysts, ACS Catal. 2 (2012) 671–683.
[15] L.J. Malobela, J. Heveling, W.G. Augustyn, L.M. Cele, Nickel–Cobalt on carbonaceous supports for the selective catalytic hydrogenation of cinnamaldehyde, Ind. Eng. Chem. Res. 53 (2014) 13910–13919.
[16] B. Viswanathan, K.R. Krishnamurthy, R. Mahalakshmi, M.G. Prakash, Selective hydrogenation of cinnamaldehyde on nickel nano particles supported on titania—role of catalyst preparation methods, Catal. Sci. Technol. 5 (2015) 3313–3321.
[17] R. Hudson, G. Hamasaka, T. Osako, Y.M.A. Yamada, C.-J. Li, Y. Uozumi, A. Moores, Highly efficient iron(^{0}) nanoparticle-catalyzed hydrogenation in water in flow, Green Chem. 15 (2013) 2141.
[18] X. Wang, P. Clark, S.T. Oyama, Synthesis, characterization, and HydrotreatingActivity of several iron group transition metal phosphides, J. Catal. 208 (2002) 321–331.
[19] Y. Shu, S.T. Oyama, A new type of nonsulfide hydrotreating catalyst: nickel phosphide on carbon, Chem. Commun. 0 (2005) 1143–1145.
[20] Y. Lee, S. Oyama, Bifunctional nature of a SiO_2-supported Ni_2P catalyst for hydrotreating: EXAFS and FTIR studies, J. Catal. 239 (2006) 376–389.
[21] S.T. Oyama, T. Gott, H. Zhao, Y.-K. Lee, Transition metal phosphide hydroprocessing catalysts: a review, Catal. Today 143 (2009) 94–107.
[22] S. Carenco, A. Leyva-Pérez, P. Concepción, C. Boissière, N. Mézailles, C. Sanchez, A. Corma, Nickel phosphide nanocatalysts for the chemoselective hydrogenation of alkynes, Nano Today 7 (2012) 21–28.
[23] W. Bonrath, T. Müller, L. Kiwi-Minsker, A. Renken, I. Iourov, Hydrogenation Process of Alkynols to Alkenols in the Presence of Structured Catalysts Based on Sintered Metal Fibers, 2011. WO2011092280., (2011).
[24] D.C. Costa, A.L. Soldati, G. Pecchi, J.F. Bengoa, S.G. Marchetti, V. Vetere, Preparation and characterization of a supported system of $Ni_2P/Ni_{12}P_5$ nanoparticles and their use as the active phase in chemoselective hydrogenation of acetophenone, Nanotechnology 29 (2018) 215702.
[25] M. Grün, K.K. Unger, A. Matsumoto, K. Tsutsumi, Novel pathways for the preparation of mesoporous MCM-41 materials: control of porosity and morphology, Microporous Mesoporous Mater. 27 (1999) 207–216.
[26] R. Xu, Particle Characterization: Light Scattering Methods, Springer Netherlands, 2002. www.springer.com/us/book/9780792363002.
[27] C.G. Granqvist, R.A. Buhrman, Ultrafine metal particles, J. Appl. Phys. 47 (1976) 2200–2219.
[28] S. Mourdikoudis, L.M. Liz-Marzán, Oleylamine in nanoparticle synthesis, Chem. Mater. 25 (2013) 1465–1476.
[29] S. Chen, X. Zhang, Q. Zhang, W. Tan, Trioctylphosphine as both solvent and stabilizer to synthesize CdS nanorods, Nanoscale Res. Lett. 4 (2009) 1159–1165.
[30] H. Guo, Y. Chen, H. Ping, J. Jin, D.-L. Peng, Facile synthesis of Cu and Cu@Cu–Ni nanocubes and nanowires in hydrophobic solution in the presence of nickel and chloride ions, Nanoscale 5 (2013) 2394–2402.
[31] T. Sreethawong, K.W. Shah, S.-Y. Zhang, E. Ye, S.H. Lim, U. Maheswaran, W.Y. Mao, M.-Y. Han, Optimized production of copper nanostructures with high yields for efficient use as thermal conductivity-enhancing PCM dopant, J. Mater. Chem. A. 2 (2014) 3417–3423.
[32] S. Carenco, C. Boissière, L. Nicole, C. Sanchez, P. Le Floch, N. Mézailles, Controlled design of size-tunable monodisperse nickel nanoparticles, Chem. Mater. 22 (2010) 1340–1349.
[33] K. Senevirathne, A.W. Burns, M.E. Bussell, S.L. Brock, Synthesis and characterization of discrete nickel phosphide nanoparticles: effect of surface ligation chemistry on catalytic hydrodesulfurization of thiophene, Adv. Funct. Mater. 17 (2007) 3933–3939.
[34] H. Winnischofer, T.C.R. Rocha, W.C. Nunes, L.M. Socolovsky, M. Knobel, D. Zanchet, Chemical synthesis and structural characterization of highly disordered Ni colloidal nanoparticles, ACS Nano 2 (2008) 1313–1319.
[35] J. Smith, Characterization of Ni/TiO_2 catalysts by TEM, X-ray diffraction, and chemisorption techniques, J. Catal. 68 (1981) 270–285.
[36] S. Oyama, Effect of phosphorus content in nickel phosphide catalysts studied by XAFS and other techniques, J. Catal. 210 (2002) 207–217.
[37] J. Ren, J. Wang, J. Li, Y. Li, Density functional theory study on crystal nickel phosphides, J. Fuel Chem. Technol. 35 (2007) 458–464.
[38] I.V. Deliy, I.V. Shamanaev, E.Y. Gerasimov, V.P. Pakharukova, I.V. Yakovlev, O.B. Lapina, P.V. Aleksandrov, G.A. Bukhtiyarova, HDO of methyl palmitate over silica-supported Ni phosphides: insight into Ni/P effect, Catalysts 7 (2017) 298.
[39] C.-S. Chen, H.-W. Chen, W.-H. Cheng, Study of selective hydrogenation of acetophenone on Pt/SiO_2, Appl. Catal. Gen. 248 (2003) 117–128.
[40] K. Li, R. Wang, J. Chen, Hydrodeoxygenation of anisole over silica-supported Ni_2P, MoP, and NiMoP catalysts, Energy Fuel. 25 (2011) 854–863.